Research article

Anti-angiogenic activity of a novel angiostatin-like plasminogen fragment produced by a bacterial metalloproteinase

Kosuke Shimizu [a,b], Naoko Nishimura [b], Taolin Wang [a], Tetsuro Yamamoto [c], Eriko Suzuki [a], Keiji Hasumi [a,b,*]

[a] Department of Applied Biological Science, Tokyo University of Agriculture and Technology, 3-5-8 Saiwaicho, Fuchu, Tokyo, 183-8509, Japan
[b] Division of Research and Development, TMS Co., Ltd., 1-9-11F Fuchucho, Fuchu, Tokyo, 183-0055, Japan
[c] Research Center, EPS Innovative Medicine, Kagurazaka AK Building, 1-8 Tsukudo-cho, Shinjuku-ku, Tokyo, 162-0821, Japan

ABSTRACT

Tumor growth depends on angiogenesis, a process by which new blood vessel are formed from pre-existing normal blood vessels. Proteolytic fragments of plasminogen, containing varying numbers of plasminogen kringle domains, collectively known as angiostatin, are a naturally occurring inhibitor of angiogenesis and inhibit tumor growth. We have developed an "affinity-capture reactor" that enables a single-step method for the production/purification of an angiostatin-like plasminogen fragment from human plasma using an immobilized bacterial metalloproteinase. The resulting fragment, named BL-angiostatin, contains one or two glycosyl chains and the N-terminal PAN module, which are not present in canonical angiostatins tested for cancer treatment. BL-angiostatin inhibited angiogenesis *in vitro* at 20 nM and the growth of both allograft and human xenograft tumors as well as lung metastasis of primary tumors mice at 0.3–10 mg kg^{-1}. Derivatives of BL angiostatin lacking the PAN module or the terminal sialic acids in the glycosyl chains showed reduced anti-angiogenic activity *in vivo*, suggesting a role for these functions in activity, possibly via conferring a pharmacokinetic advantage to BL angiostatin compared to recombinant angiostatin lacking both features. These results highlight the potential of BL-angiostatin for therapeutic applications.

1. Introduction

Angiostatin, a proteolytic fragment of plasminogen, is a naturally occurring inhibitor of angiogenesis and suppresses tumor growth [1,2]. Several proteases including matrix metalloproteinases [3,4], a metalloelastase [5,6], and tissue kallikreins [7,8], as well as plasmin autoproteolysis [9–11] can be involved in the generation of angiostatin from plasminogen. Angiostatin targets several molecules including cell surface F1-Fo ATP synthase [12], angiomotin [13], integrins [14], annexin II [15], resulting in inhibition of endothelial cell migration/proliferation and induction of apoptosis [16].

Native angiostatin occurs in some glycoforms, and a specific form of Thr^{346}-O-glycosylation may influence angiostatin activity [17]. The production of natural glycoform angiostatin can be achieved by proteolytic cleavage of plasminogen, which requires plasminogen purification, a limited proteolytic cleavage using a suitable protease, and purification of the resulting angiostatin, which

Abbreviations

Asialo-BLAS a BL-angiostatin derivative lacking sialic acids at the termini of glycosyl chains
AUC   area under the drug concentration-time curve
BLAS   BL-angiostatin
BLMA   bacillolysin MA
DAS   dorsal air sack
DesPAN-BLAS a BL-angiostatin derivative lacking the N-terminal PAN module
HE   hematoxylin-eosin
HUVEC   human umbilical vein endothelial cells
IQR   interquartile range
LLC   Lewis lung carcinoma
S180   mouse sarcoma-180
SEM   standard error of the mean
$t_{1/2}$ half-life
VEGF   vascular endothelial growth factor

require careful quality control [2] and limit its use to production for a therapeutic use. Recombinant angiostatins have been developed and tested for safety and efficacy [19,20], whereas recombinant angiostatins are not yet approved, possibly because of concerns about efficacy.

We have developed an "affinity-capture reactor" that allows a single-step method for the production/purification of an angiostatin-
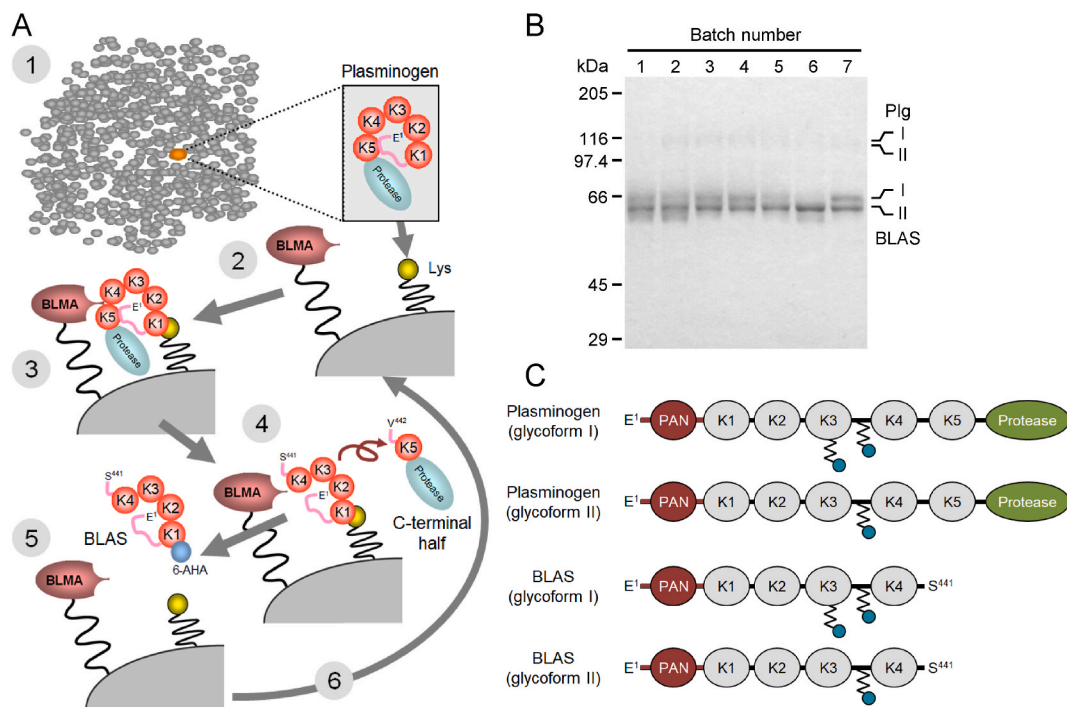
Fig. 1. Production/purification of BLAS using the BLMA/Lys affinity-capture reactor. (A) Diagram showing the production/purification of BLAS using the BLMA/Lys affinity-capture reactor, where: (1) plasminogen comprises 0.25 % of other plasma proteins which may prevent specific proteolysis of plasminogen to form angiostatin; (2) the reactor captures/concentrates plasminogen via the lysine moiety, (3) allowing plasminogen cleavage by the co-immobilized BLMA; (4) BLAS, the resulting N-terminal fragment, is retained on the reactor, and the C-terminal fragment is washed away; (5) BLAS is recovered by elution with 6-aminohexanoic acid; and (6) the reactor can be used repeatedly for long periods of time. Reproduced from ref. 20. (B) Representative results of the production/purification of BLAS. A result of reduced SDS-polyacrylamide gel (7.5 %) electrophoresis analysis of samples obtained from 7 cycles of the reactor operation is shown. Uncropped gel image is provided as a supplementary material (Uncropped gel image for Fig. 1B). (C) Schematic representation of the structure of BLAS. Human plasminogen exists in two glycoforms: glycoform I, which contains both Asn^{289}-N-linked and Thr^{346}-O-linked oligosaccharides, and glycoform II, which contains only the latter. Thus, the BLAS molecule resulting from the affinity-capture reactor process consists of two glycoforms corresponding to the respective plasminogen glyco-forms. The zigzag line represents an oligosaccharide chain, and the circle at the end of the zigzag line represents sialic acid(s). Each of the plasmin domains is shown as a circle with a caption.

like plasminogen fragment from human plasma using an immobilized bacterial metalloproteinase [20]. The reactor consists of bacillolysin-MA (BLMA) [21] as a protease for specific plasminogen cleavage and lysine as an affinity ligand for plasminogen capture, allowing plasminogen concentration/cleavage and purification of the resulting angiostatin fragment (designated BL-angiostatin; BLAS) simultaneously [19]. BLAS contains the natural glycosyl chain(s) of plasminogen as well as the N-terminal PAN module, making BLAS unique among the reported angiostatins [20].

In this paper, we describe the anti-angiogenic activities of BLAS, suggesting a role for sialic acid residues at the termini of glycosyl chains and the PAN module of BLAS in anti-angiogenic activity *in vivo*. In addition, we report the antitumor and anti-metastatic potentials of BLAS and the use of BLMA for the *in vivo* generation of BLAS-like plasminogen fragments in mice. Recent studies have implicated angiostatin in the modulation of endothelial dysfunction, dementia, and inflammation [22–26]. Our data highlight the potential for the use of BLAS in the treatment of cancer and these diseases.

2. Materials and methods

2.1. Materials

BLMA was purified from a culture of *Bacillus megaterium* A9542 as described previously [5]. The BLMA/Lys affinity-capture reactor was prepared by immobilizing BLMA on HiTrap NHS-activated HP (Cytiva, Tokyo, Japan), followed by coupling with lysine to allow plasminogen binding to the beads [20]. Briefly, one volume of HiTrap NHS-activated HP, pre-equilibrated with buffer A (0.1 M NaHCO$_3$, 0.5 M NaCl and 0.65 M isopropanol, pH 8.3) was incubated with two volumes of BLMA solution (0.2 mg ml^{-1} in buffer A) for 2 h at room temperature. After draining the enzyme solution, the gel was further incubated with two volumes of 0.2 M lysine in 0.65 M isopropanol, aq, pH 8, for 2 h at room temperature. Finally, the gel was washed with 50 vol of buffer B (25 mM sodium phosphate and 0.65 M isopropanol, pH 7.4) and stored in buffer B containing 3.1 mM sodium azide at 4 °C until use. Human citrated plasma was kindly provided by the Tokyo-Nishi Red Cross Blood Center (Tachikawa, Japan). Mouse Lewis lung carcinoma (LLC; TKG 0153), mouse sarcoma-180 (S180; TKG 0173), human colorectal carcinoma COLO 205 (TKG 0457), and human prostate cancer PC-3 (TKG 0600) cell lines obtained from the Cell Resource Center for Biomedical Research, Institute of Development, Aging and Cancer, Tohoku University (Sendai, Japan), and human ovarian adenocarcinoma SK-OV-3 cell line (HTB-77), obtained from ATCC (Manassas, VA, USA), were cultured according to the supplier's recommendations.

2.2. Production/purification of BLAS using the BLMA/Lys affinity-capture reactor

The BLMA/Lys affinity-capture reactor was operated at 4 °C as follows (see a schematic diagram of the affinity capture process in Fig. 1A). Human citrated plasma containing 0.65 M isopropanol was centrifuged at 15,000×*g* for 20 min. The resulting supernatant (90 mL) was added to a 10-mL reactor pre-equilibrated with buffer B for 1 h. The reactor was washed with 300 mL of buffer B containing 0.5 M NaCl for 1.5 h. BLAS was eluted with 50 mL of 0.2 M 6-aminohexanoic acid containing 0.65 M isopropanol for 0.5 h, and 10-mL fractions of the eluate were collected. BLAS was recovered from the second and third fractions.

2.3. Preparation of BLAS derivatives

We prepared a BLAS derivative lacking the N-terminal PAN module (desPAN-BLAS) and that lacking sialic acids at the ends of glycosyl chains (asialo-BLAS) by treating BLAS with HiTrap NHS-activated HP coupled with plasmin and exosialidase, respectively (plasmin cleaves the Lys^{77}−Lys^{78} bond, dissociating the N-terminal PAN module from the main body of the BLAS molecule). Briefly, 1 mg of human plasmin (Wako Pure Chemical, Osaka, Japan) was coupled to 1 mL of HiTrap NHS-activated HP according to the standard method used for BLMA coupling (see above), except that lysine was not included in the coupling reaction. Neuraminidase (5 units) from *Arthrobacter ureafaciens* containing α2-3,6,8 exo-neuraminidase activities (Nacalai Tesque, Kyoto, Japan), was coupled to 1 mL of HiTrap NHS-activated HP in buffer B without isopropanol, followed by blocking with monoethanolamine. BLAS (1 mg mL^{-1}; 3 mL) was applied to the plasmin-immobilized column pre-equilibrated with buffer C (50 mM Tris-HCl, pH 7.4, 100 mM NaCl, 0.01 %, wt/vol, Tween 80) at a rate of 1 mL min^{-1} at 28 °C, followed by an elution with 2 mL of buffer C. For the neuraminidase-coupled column, BLAS (3 mg mL^{-1}; 2 mL) was applied in buffer D (0.1 M Na-acetate, pH 5.4, 0.1 M lysine, and 2 mM CaCl$_2$) at a rate of 1 mL min^{-1} at 28 °C, followed by an elution with 1 mL of buffer D. Fractions containing good purity were pooled. The amount of sialic acid released was determined using a fluorescence labelling kit (Takara Bio, Kusatsu, Japan).

2.4. In vitro angiogenesis assay

We assayed *in vitro* angiogenesis using a coculture of primary human umbilical vein vascular endothelial cells (HUVEC) and human dermal fibroblast cells using a commercial kit (KZ-1000, Kurabo, Osaka, Japan), in which the coculture was provided in a 24-well plate format. The medium was refreshed on days 1, 2, 4, 7, and 9. BLAS, at 0, 2, 20, or 200 nM, and vascular endothelial growth factor (VEGF), at 10 ng mL^{-1} (KZ-1350, Kurabo), were added to in each medium. As a control, cells were incubated with medium containing neither BLAS nor VEGF was performed. On day 11, endothelial tubes were stained with anti-CD31 antibody (KZ-1225, Kurabo) after fixation in 70 % ethanol according to the manufacturer's instructions.

2.5. Animal experiments

Animal studies were performed at the Tokyo University of Agriculture and contract laboratories, New Drug Research Laboratories (Eniwa, Japan), Panapharm Laboratories (Uto, Japan), and Daiichi Pure Chemical (Tokyo, Japan). Animal protocols were approved by the Tokyo Noko University Animal Experiment Subcommittee or by the institutional review board of the contract laboratories. Animals were housed in a climate-controlled animal facility, maintained at a temperature of 23 ± 2 °C and a relative humidity of 50 ± 20 %, with a structured 12-h light/dark cycle, with the light phase of 8:00 a.m. to 8:00 p.m. Animals were given ad libitum access to standard chow and water. Crlj:CD1 (ICR) mice, Crl:CD (SD) rats, and CAnN.Cg-$Foxn1^{nu}$/CrlCrlj nude mice were obtained from Charles River Japan (Yokohama, Japan). Slc:BDF1, KSN/Slc, and BALB/cSlc-nu/nu mice were obtained from Japan SLC (Hamamatsu, Japan). C57BL/6J mice were obtained from CLEA Japan (Tokyo, Japan) and Sankyo Labo Service (Tokyo Japan). Animals were assigned to groups after $7-9$ days of acclimation.

2.6. Assessment of acute toxicity in mice

On day 0, six-week-old male and female Crlj:CD1 (ICR) mice ($n = 5$) were intravenously administered vehicle (saline; 10 mL kg^{-1}) or BLAS at 100 mg kg^{-1} via a tail vein. General condition was observed daily. On day 14, pathological and anatomical examinations were performed on organs and tissues of the head and thorax/abdomen; the brain, lungs, heart, liver, stomach, intestines, spleen, pancreas, kidneys, urinary bladder, and genital organs.

2.7. Plasma ^{125}I-BLAS kinetics in rats

BLAS was iodinated with Na^{125}I using the IODO-GEN method as described previously [21]. The resulting ^{125}I-BLAS had a specific radioactivity of 46.2 cpm ng^{-1}, with 92.3 % of the radioactivity being trichloroacetic acid-precipitable. Eight-week-old Crl:CD (SD) male rats received an intravenous injection of ^{125}I-BLAS at 1 mg kg^{-1} from the tail vein ($n = 3$). Blood (250 μL) was collected in sodium citrate at 0.083, 0.25, 0.5, 1, 2, 4, 8, 10, 24, and 48 h after the injection to determine total and trichloroacetic acid-precipitable radioactivity. The plasma level of radioactivity was calculated from the trichloroacetic acid-precipitable radioactivity.

2.8. Evaluation of angiogenesis in vivo using a dorsal air sack (DAS) model in mice

A chamber consisting of two Millipore filters (0.45 μm), which were attached to either side of a 1-cm Millipore ring using Millipore MF cement [27], was filled with 5×10^6 mouse sarcoma-180 (S180) cells. The resulting chamber was implanted into a DAS created by injecting 10 mL of air into the back of nine-week-old Crlj:CD-1 (ICR) female mice (day 0). As a negative control, chambers without tumor cells were used. In the first experiment, saline or BLAS (1 and 10 mg kg^{-1}) was administered intravenously once a day from day 0 to day 4 to mice bearing S180-encapsulated chambers ($n = 10$ in each group). In the second experiment, saline, BLAS (0.8 and 8 mg kg^{-1}), DesPAN-BLAS (0.8 and 8 mg kg^{-1}), or asialo-BLAS (0.8 and 8 mg kg^{-1}) was administered intravenously once daily from day 0 to day 4 ($n = 6$ in each group). Negative control animals received saline alone. On day 5, the chamber was removed under anesthesia, and meandering vessels ≥ 3 mm in length were counted at the DAS chamber contact area on the skin as an index of angiogenesis.

2.9. Evaluation of tumor growth in a syngeneic mouse model

Six-week-old male Slc:BDF1 mice received 1×10^5 LLC cells subcutaneously on the ventral side. Saline or BLAS at a dose of 10 mg kg^{-1} in a volume of 5 mL kg^{-1} ($n = 8$ for each group) was administered intravenously via the tail vein once daily for 14 days starting from the day after the tumor implantation (day 0). On day 15, animals were sacrificed under ether anesthesia, and in situ tumors were resected. Tumors from three randomly selected animals in the control, 3 mg kg^{-1}, and 10 mg kg^{-1} groups were processed for histopathological analysis after hematoxylin-eosin (HE) staining and von Willebrand factor immunostaining.

2.10. Evaluation of tumor growth in xenograft models in nude mice

Six-week-old KSN/Slc and BALB/cSlc-nu/nu male mice received 5×10^5 of COLO 205 and PC-3 cells, respectively, subcutaneously on the ventral side. Saline or BLAS at a dose of 10 mg kg^{-1} in a volume of 5 mL kg^{-1} ($n = 8$ for each group) was administered intravenously via the tail vein once daily for 14 days starting from the day after the tumor implantation (day 0). On day 15, animals were sacrificed under ether anesthesia, and in situ tumors were resected. In another experiment, seven-week-old CAnN.Cg-$Foxn1^{nu}$/ CrlCrlj female nude mice received 5×10^6 of SK-OV-3 cells subcutaneously on the back (day 0). On day 1, an osmotic pump (Alzet 1002, DURECT, Cupertino, CA, USA) containing saline or BLAS was implanted subcutaneously in each mouse ($n = 8$ for each group). The rate of fluid release from the pump was 6 μL per day, and the dose of BLAS was 3 mg kg^{-1}. The osmotic pump was replaced every two weeks. On day 71, animals were sacrificed under CO$_2$ anesthesia, and tumors were resected. Tumors of representative size in each group were processed for histopathological analysis after HE staining and CD31 immunostaining.

2.11. Evaluation of tumor metastasis in mice

Six-week-old male CS7BL/6J mice received 1×10^6 of LLC cells subcutaneously near the right forelimb. When the size of the

implanted tumor reached to ~1000 mm^3 in volume, the primary tumor was resected. The next day (day 1), the animals were assigned to groups based on the size of the primary tumor to ensure that the mean tumor size of each group was balanced. Saline or BLAS (0.3 and 3 mg kg^{-1}) was intraperitoneally administered to each animal once daily from day 1 to day 17 ($n = 12$ for each group). The normal animal group ($n = 5$) did not undergo tumor implantation or intraperitoneal injection. Mice found to be moribund during this period (2 in the control, 2 in the BLAS 3 mg kg^{-1}, and 3 in the BLAS 3 mg kg^{-1} groups) were excluded. On day 18, animals were sacrificed under ether anesthesia, and the lungs were harvested and processed for histological analysis after HE staining to determine metastatic area versus total lung area from microscopic images.

2.12. In vivo generation of plasminogen fragments in mice after BLMA injection

Six-week-old male CS7BL/6J mice were given an intravenous injection of saline (5 mL kg^{-1}) or BLMA at the indicated doses or saline. At the indicated times, blood was collected from the vena cava under an isoflurane anesthesia in trisodium citrate, phenyl-methylsulfonyl fluoride (10 mM), and an inhibitor cocktail P8340 (Sigma-Aldrich, Darmstadt, Germany). Aliquots of the resulting plasma (1 μL) were resolved by nonreduced SDS-polyacrylamide gel electrophoresis on a 7.5 % gel. The gel was processed for immunoblotting using rabbit anti-mouse plasminogen antibody and horseradish peroxidase-conjugated anti-rabbit IgG (BioLegend, San Diego, CA, USA).

2.13. Data analysis

Data are expressed as the mean ± standard error of the mean (SEM) or the median and interquartile range (IQR). Statistical significance was tested using the Kruskal-Wallis test followed by the Shirley-Williams test or the nonparametric Dunnett's test with a joint ranking method for multiple comparisons with the control group, and the Brunner-Munzel test for comparison between two groups. P values less than 5 % were considered significant. For the Shirley-Williams test, test statistics exceeding a 5 % critical value were considered significant. Where mentioned, outliers detected by the Smirnov-Grubbs rejection test were excluded from the analyses.

3. Results

3.1. Production/purification of BLAS

A 10-mL BLMA/Lys affinity-capture reactor (Fig. 1A) yielded 4−6 mg of BLAS from 90 mL human plasma in a single cycle. The
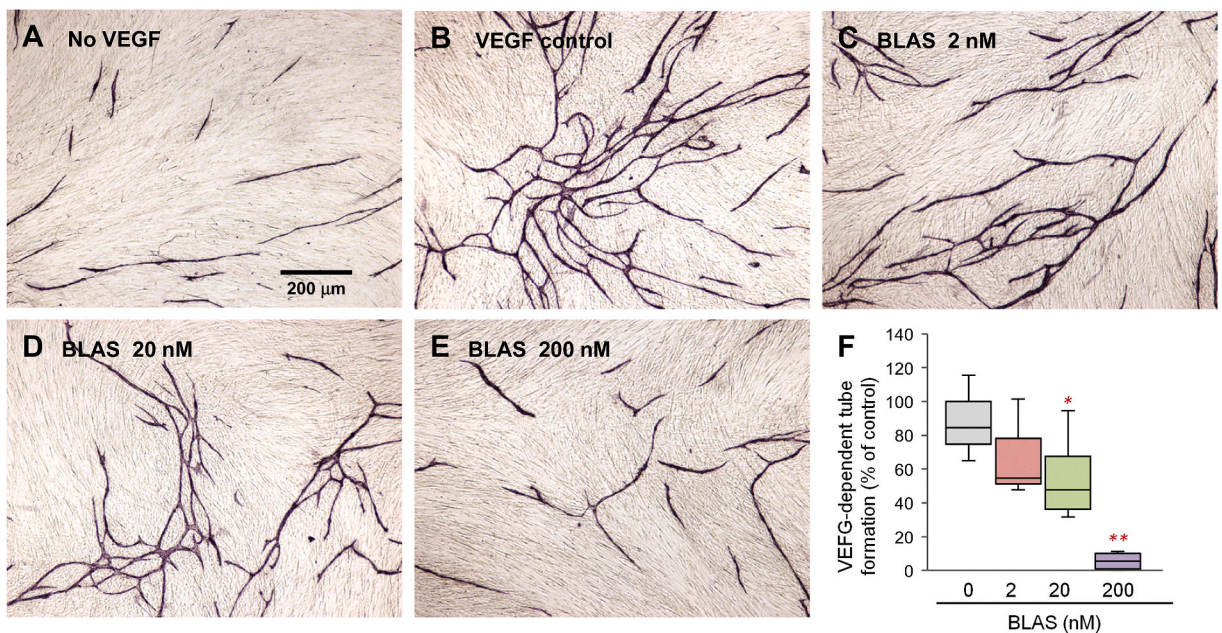
Fig. 2. BLAS inhibits angiogenesis *in vitro*. HUVEC/fibroblast cocultures were treated with VEGF (10 ng mL^{-1}) to induce tube formation. Representative microscopic images for (A) no VEGF negative control, (B) VEGF positive control, and (C–E) BLAS at 2, 20, and 200 nM added to VEGF incubations are shown. (F) The area of endothelial tubes relative to the total field area (mean ± SEM), calculated for each microscopic image from triplicate incubations in each group, is shown as a percentage of the positive control value. Bar and box represent the minimum/maximum and IQR, respectively. The median is shown as a horizontal line in the box. *, statistic >5 % critical value; **, statistic >2.5 % critical value from the Shirley-Williams test compared with the control group.

purity of the resulting BLAS was 80–95 %, with plasminogen as the major impurity, as determined by gel electrophoresis (Fig. 1B). The identity of the BLAS preparation as Glu^1-Ser^{441} of plasminogen and the presence of two glycoforms, glycoforms I and II (see Fig. 1C for schematics), was confirmed based on previous findings [20].

3.2. Inhibition of angiogenesis in vitro

The anti-angiogenic potential of BLAS was evaluated *in vitro* using a coculture system of HUVEC and human dermal fibroblasts in which tube formation was induced by VEGF (Fig. 2A and B). BLAS inhibited the VEGF-induced angiogenesis in a concentration-dependent manner (Fig. 2C−2E), achieving 50 % inhibition at ~20 nM (Fig. 2F).

3.3. Acute toxicity

As part of the safety evaluation of BLAS prior to pharmacological evaluation, the acute toxicity of a single intravenous dose was investigated in male and female mice. Compared with saline-treated controls, no changes in systemic symptoms were observed throughout the observation period from day 0 to day 14 following injection of BLAS at 100 mg kg^{-1}, which was 10–300 times higher than the pharmacological doses (see below). No changes suggestive of BLAS toxicity, including the dysfunction in the hemostatic system, such as bleeding, fibrin deposition, and blood flow obstruction, were observed at necropsy on day 14.

3.4. Plasma kinetics

Plasma levels of BLAS injected intravenously into rats appeared to decline in two phases (Fig. 3A). During the first phase, up to 4 h after dosing, a plasma half-life ($t_{1/2}$) of 1.5 ± 0.2 h was estimated from the plasma decay curve. During the second phase, from 8 to 48 h, the $t_{1/2}$ was estimated to be 23.6 ± 3.9 h, suggesting that BLAS was rapidly distributed to the central compartment, the plasma and high perfusion tissues such as the liver and kidneys, followed by distribution to other peripheral tissues where BLAS was slowly cleared. The area under the drug concentration-time curve (AUC) for the plasma BLAS was estimated to be 49.9 ± 2.1 µg eq. h mL^{-1} up to 48 h and 58.2 ± 41 µg eq. h mL^{-1} for the total AUC ($AUC_{0-\infty}$). From these data, we concluded that daily BLAS treatment could be suitable for pharmacological evaluation.
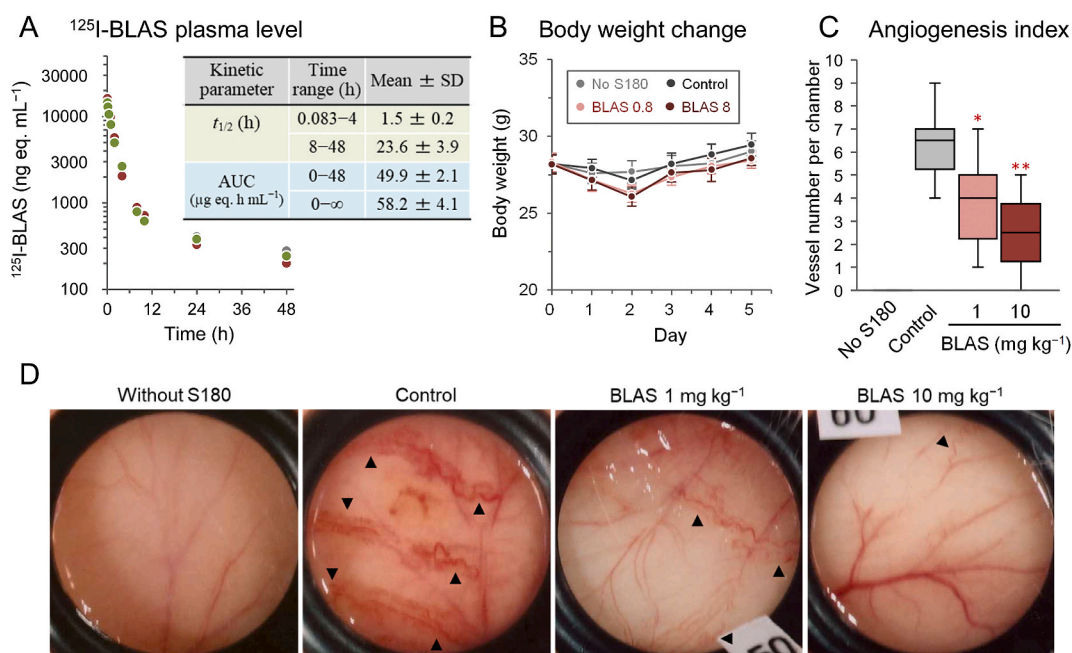
Fig. 3. BLAS inhibits angiogenesis in a murine DAS model. (A) Plasma kinetics of ^{125}I-BLAS in rats. Plasma levels of trichloroacetic acid-precipitable radioactivity were used to calculate plasma ^{125}I-BLAS levels. Data from three animals are shown. The inset shows the $t_{1/2}$ and AUC estimated from the trichloroacetic acid-precipitable radioactivity data. (B) Change in body weight during the evaluation of BLAS in a DAS angiogenesis model in mice, where saline or BLAS at the indicated doses was administered intravenously for 5 days prior to angiogenesis assessment. No S180 represents animals that received a DAS chamber without S180 cells and without BLAS treatment. (C) Summary of the angiogenic index obtained from 10 animals. Bar and box represent the minimum/maximum and IQR, respectively. The median is shown as a horizontal line in the box. *, statistic >5 % critical value; **, statistic >2.5 % critical value from the Shirley-Williams test compared with the control group. (D) Representative image for the skin surface facing the implanted DAS chamber. Arrowhead indicated newly formed meandering vessels ≥3 mm in length, which were counted as an angiogenic index.

3.5. Inhibition of angiogenesis in vivo

The effect of BLAS on tumor-induced angiogenesis was investigated using a DAS model in mice. As shown in Fig. 3C and D, mice with a DAS chamber containing mouse sarcoma-180 cells developed significantly more neovascularization (median angiogenesis index 6.5; IQR 5−7.25) than rats with a chamber containing no tumor cells (median 0; IQR 0−0). The tumor-induced angiogenesis was significantly inhibited by daily treatment with BLAS at 1 and 10 mg kg^{-1} (median 4; IQR 2.5−5, and median 2.5; IQR 0.75−4, respectively) (Fig. 3C and D) without any adverse effects on the general conditions including body weight of the treated animals (Fig. 3B).

3.6. BLAS derivatives lacking the PAN module or the terminal sialic acids in the glycosyl chains show reduced anti-angiogenic activity *in vivo*.

DesPAN-BLAS, lacking the PAN module, and asialo-BLAS, lacking the terminal sialic acids in the glycosyl chains, were prepared to evaluate the role of these moieties in the anti-angiogenic activity of BLAS (see Fig. 4A for schematics). The gel electrophoresis results showed the loss of molecular mass corresponding to the PAN module in desPAN-BLAS (Fig. 4A). In the asialo-BLAS preparation, the apparent molecular mass changed slightly, and a removal of 2.7 mol of sialic acids per mole of BLAS was estimated from the sialic acid analysis. These derivatives showed lower activities compared to native BLAS in the DAS angiogenesis model (Fig. 4C). BLAS inhibition of tumor-induced angiogenesis was significant at 0.8 mg kg^{-1} compared to saline control (median angiogenesis index 3.5; IQR 3−4. 25 vs. median 6; IQR, 6−9), whereas inhibition by desPAN-BLAS and asialo-BLAS was insignificant at 0.8 mg kg^{-1} (median 4; IQR 3−4. 25 and median 6; IQR, 4−7, respectively). In addition, asialo-BLAS failed to achieve significant inhibition at 8 mg kg^{-1} (median 3; IQR 1−6). All doses had no effect on the general condition or body weight of the treated animals (Fig. 4B).

3.6. Suppression of tumor growth in a syngeneic implantation model

BLAS was effective in suppressing the growth of LLC implanted subcutaneously in BDF1 mice. BLAS, at a dose of up to 10 mg kg^{-1} per day, did not affect body-weight gain, compared to the saline-treated control group during the 15-day treatment period (Fig. 5A). In the control group, tumors were visible from day 8 after the tumor implantation. BLAS significantly suppressed the growth of tumor
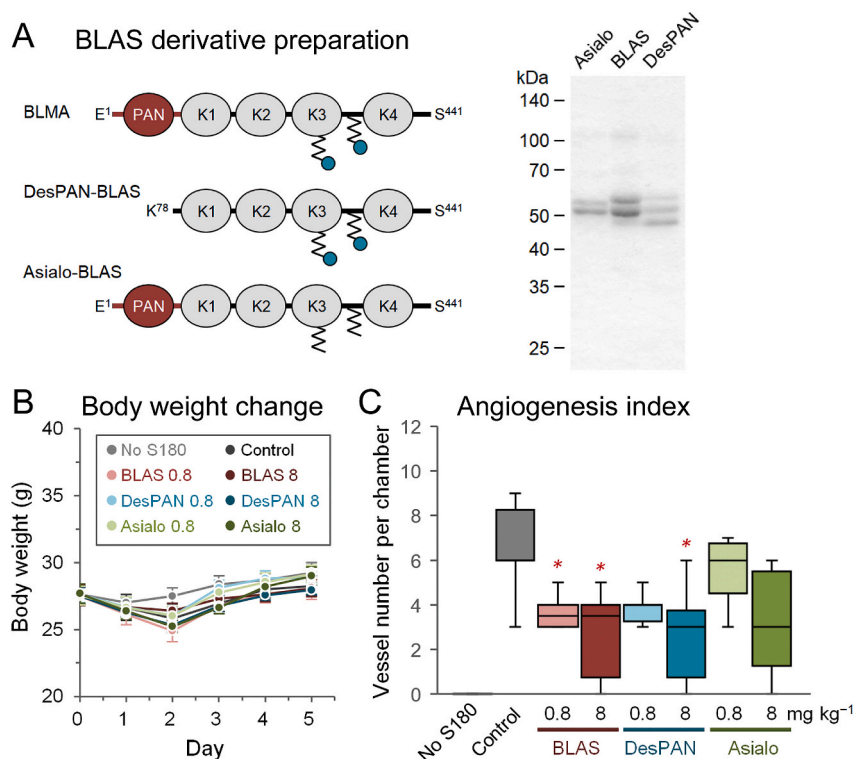
Fig. 4. The PAN module and the terminal sialic acids in the glycosyl chains affect BLAS activity in a murine DAS angiogenesis model. (A) Preparation of DesPAN-BLAS and asialo-BLAS. Schematics of the structures of BLAS and its derivatives are shown on the left (see legend to Fig. 1 for symbols). For simplicity, only glycoform I is shown. The right panel shows the result of reduced SDS-polyacrylamide gel (7.5 %) electrophoresis analysis of the derivatives compared to native BLAS. Uncropped gel image is provided as a supplementary material (Uncropped gel image for Fig. 4A). (B) Change in body weight during the DAS assay. (C) Summary of the angiogenic index obtained from 6 animals. Bar and box represent the minimum/maximum and IQR, respectively. The median is shown as a horizontal line in the box. *, $P < 0.05$ by the nonparametric Dunnett's test with a joint ranking method compared with the control group.
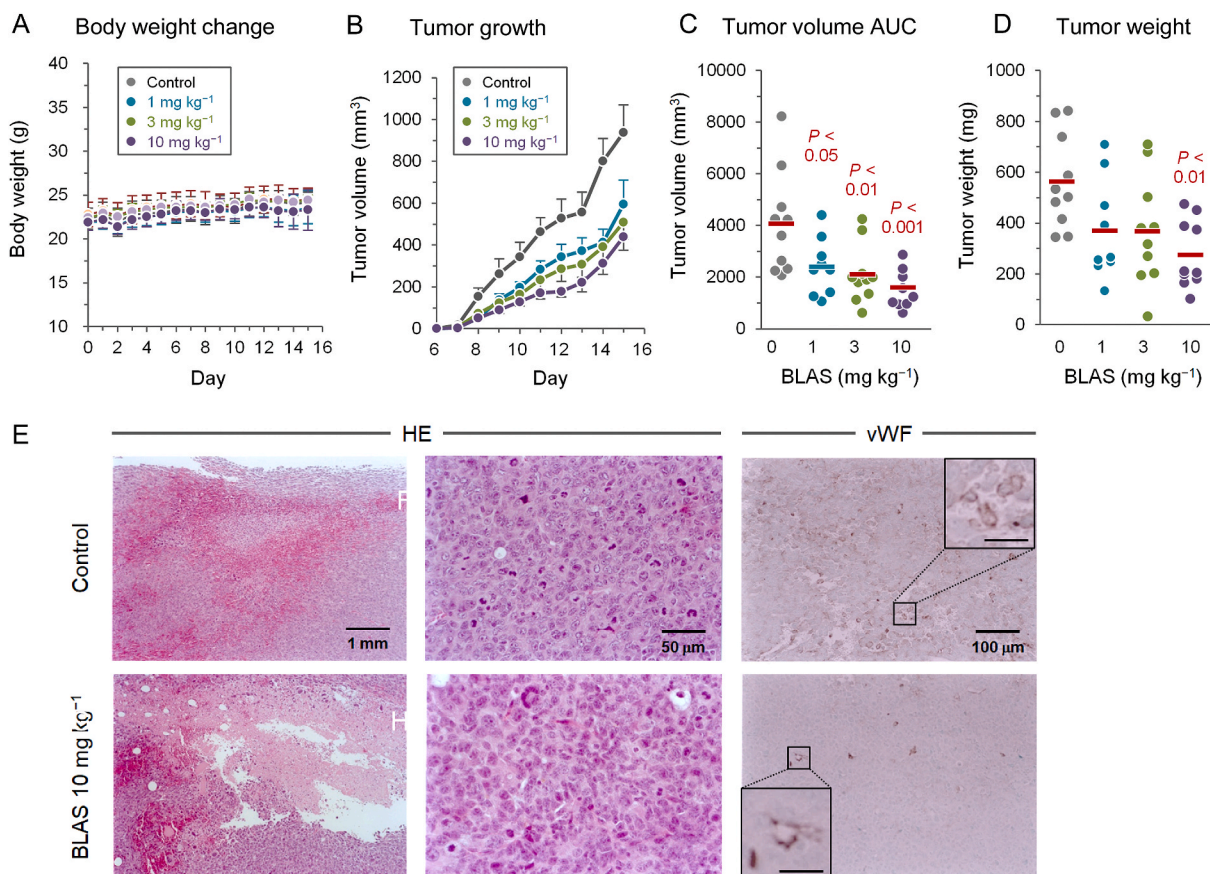
Fig. 5. BLAS inhibits tumor growth in a syngeneic mouse implantation model. LLC-bearing BDF1 mice were treated with intravenous BLAS at the indicated doses for 14 days. (A) Change in body weight over the treatment period. (B) Change in tumor volume. (C) Tumor volume AUC, which reflects total tumor growth for comparisons between groups [45]. (D) Tumor weight on day 15. (E) Representative images of tumor sections stained with HE and with anti-von Willebrand factor (vWF) antibody. Inset shows a high-power image, with a scale bar representing 25 μm. The number of animals from which data were analyzed was 10 in all groups except 8 in the 1 mg kg^{-1} group, where 2 outliers were eliminated by the Smirnov-Grubbs rejection test. Bar and box represent the minimum/maximum and IQR, respectively. Median is shown as a horizontal line in the box. *, statistic >5 % critical value; **, statistic >2.5 % critical value from the Shirley-Williams test compared with the control group.

after daily intravenous injection at 0.3 mg kg^{-1} or more, as assessed by tumor volume (Fig. 5B and C) and tumor weight (Fig. 5D). The HE staining and anti-vWF staining of tumor sections (Fig. 5E) indicated that BLAS treatment resulted in extensive necrosis (left panel), reduced tumor cell division (middle panel), and sparse blood vessels (right panel) compared to the control group.

3.7. Suppression of tumor growth in xenograft models

The antitumor activity of BLAS was confirmed in xenograft models in which human cancer cell lines were implanted in nude mice. At an intravenous dose of 10 mg kg^{-1} per day, BLAS significantly suppressed the growth of the human colorectal cancer line COLO 205 (Fig. 6A) and the human prostate cancer line PC-3 (Fig. 6B). BLAS delivered via a subcutaneous osmotic pump was also effective in suppressing the growth of the human ovarian cancer SK-OV-3 line (Fig. 6C), which was associated with extensive necrosis and sparse blood vessels (Fig. 6D), compared to the control group. Under these conditions, BLAS had no effect on general conditions or body weight gain.

3.8. Suppression of tumor metastasis

The effect of BLAS on tumor metastasis was evaluated in mice with subcutaneously implanted LLC after resection of the primary tumor. The median lung weight of the control mice receiving saline was 0.282 g (IQR 0.202−0.321 g), compared to the lungs of normal mice (median 0.152 g; IQR 0.146−0.176 g). In the mice receiving intraperitoneal BLMA, median lung weights were 0.181 g (IQR 0.169−0.304 g) and 0.157 g (IQR 0.142−0.181 g) in the 0.3 mg kg^{-1} and 3 mg kg^{-1} groups, respectively (Fig. 7A). The increase in the lung weights was associated with metastatic growth of the tumor. The metastatic area relative to the total lung area in BLAS-treated mice (median 11.0 %; IQR 5.8−11.7 % and median 11.0 %; IQR 5.8−11.7 % in the 0.3 mg kg^{-1} and 3 mg kg^{-1} groups, respectively)
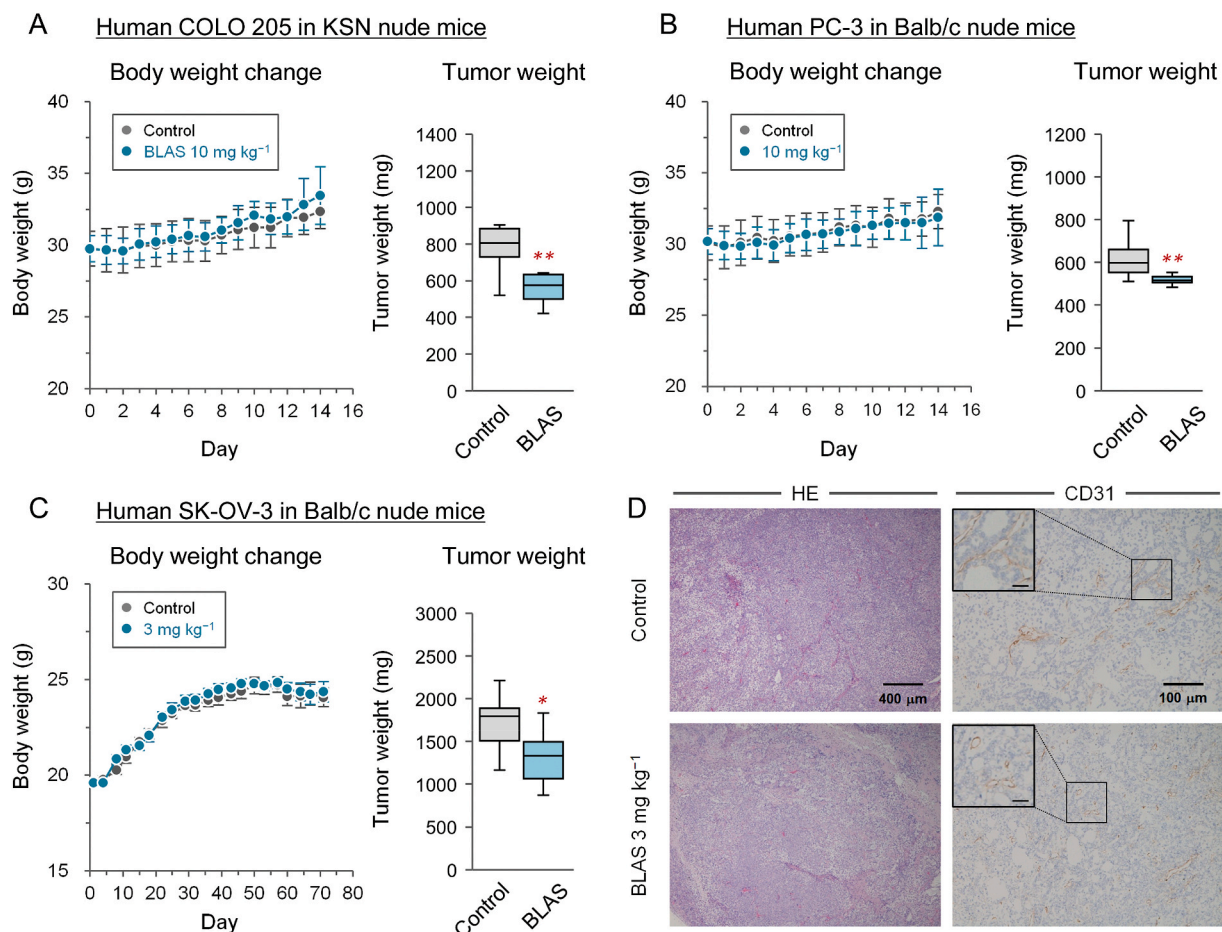
Fig. 6. BLAS inhibits tumor growth in xenograft tumor models in nude mice. Nude mice bearing human tumors were treated with BLAS at the indicated doses. (A) COLO 205-implanted KSN mice received intravenous saline or BLAS daily for 14 days, and tumor weight was determined on day 15. (B) PC-3-implanted Balb/c nude mice received intravenous saline or BLAS daily for 14 days, and tumor weight was determined on day 15. (C) SK-OV-3-implanted Balb/c nude mice received subcutaneous saline or BLAS via an osmotic pump for 70 days, and tumor weight was determined on day 71. (D) Representative images of the SK-OV-3 tumor sections stained with HE and with anti-CD31 antibody (CD31). Inset shows a high-power image, with a scale bar representing 25 μm. Bar and box represent the minimum/maximum and IQR, respectively. The median is shown as a horizontal line in the box. *, P < 0.05; **, P < 0.01 by the Brunner-Munzel test compared with the control group.

was significantly lower than that in control mice (median 20.9 %; IQR 7.7−26.6 %) (Fig. 7B and C).

3.9. In vivo generation of plasminogen fragments in mice after injection of BLMA

To test the potential of the BLAS-generating enzyme BLMA to promote angiostatin generation *in vivo*, we intravenously administered BLMA intravenously to mice and assessed the levels of plasminogen fragments in the plasma of treated animals by immunoblotting. Plasma from control animals contained small amounts of proteins with apparent molecular masses of 52 and 44 kDa that reacted with an anti-plasminogen antibody (Fig. 8). In the plasma of animals treated with BLMA for 15 min, unique proteins appeared at 37 and 42 kD, and the intensity of the 42 kDa protein increased with increasing dose of BLMA (Fig. 8A). The intensities of the 37 and 42 kD protein bands were roughly estimated to be less than 10 % of plasminogen (Fig. S1). Plasma levels of the 42 kDa protein were maintained for up to 45 min (Fig. 8B), suggesting a potential for BLMA administration to promote the generation of the BLAS-like plasminogen fragment *in vivo*.

4. Discussion

In this study, we evaluate the anti-angiogenic and antitumor potentials of BLAS, an angiostatin-like plasmin fragment produced using the affinity-capture reactor, which allows a simple, large-scale production/purification from plasma under mild conditions using the bacterial metalloproteinase BLMA. Although there are some impurities, which mainly consists of plasminogen, in the BLAS preparation, we believe that a small amount of the contaminating plasminogen (up to 0.032 μM when taking a level of 10 %
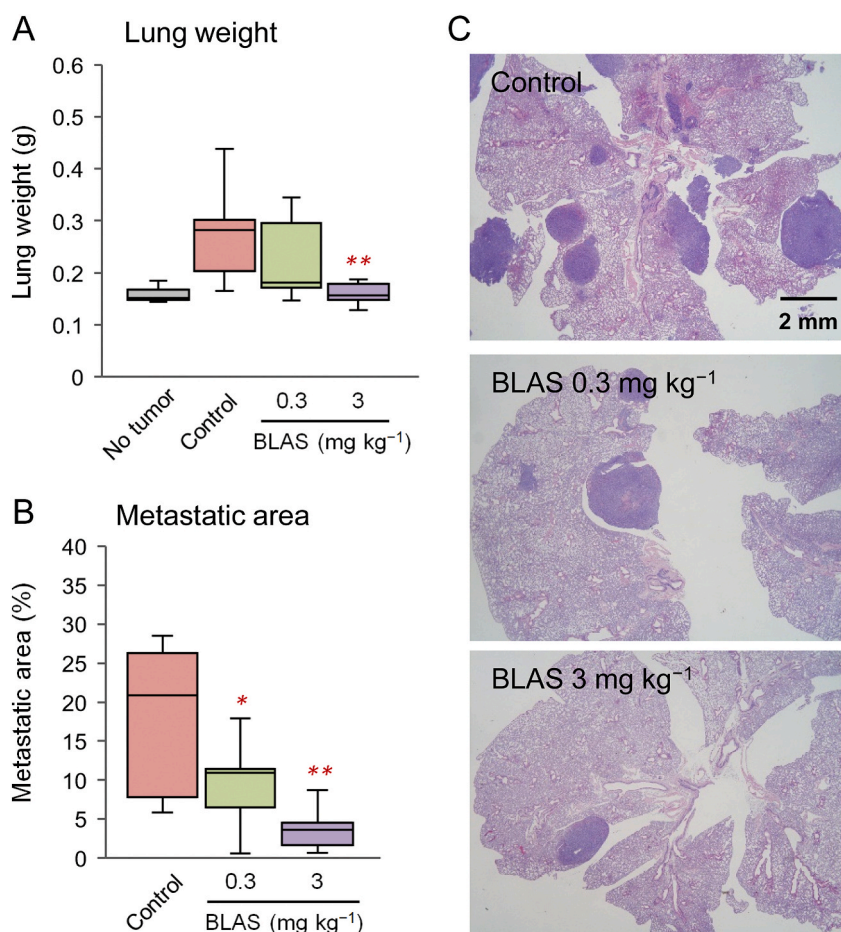
Fig. 7. BLAS inhibits tumor metastasis after primary tumor resection. Primary tumors derived from subcutaneously implanted LLC were resected when the size reached to ~1000 mm^3 in volume (day 0), and the mice received BLAS at the indicated doses daily by intraperitoneal injection daily for 17 days from day 1. (A) Wet weight of the lungs resected on day 18, and (B) tumor metastatic area calculated from microscopic images of the lung sections stained with HE. The number of animals from which data were analyzed was 9, 8, and 7 in the control, the 0.3 mg kg^{-1}, and the 3 mg kg^{-1} groups, respectively, after eliminating outliers by the Smirnov-Grubbs rejection test based on the lung weight ($n = 1$, 2, and 2, respectively, in each group). Metastatic area data were not available for one animal in each of the control and the 0.3 mg kg^{-1} groups. Bar and box represent the minimum/maximum and IQR, respectively. The median is shown as a horizontal line in the box. *, statistic >5 % critical value; **, statistic >2.5 % critical value from the Shirley-Williams test compared with the control group. (C) Representative images of the HE-stained lung sections where metastatic lesions were heavily stained with hematoxylin.

contamination in the BLAS given at a pharmacological dose of 1 mg kg^{-1}, which gives rise to a plasma BLAS concentration of 0.32 μM = 16 μg mL^{-1}, Fig. 2A) may have no effect taking that this level accounts for 1.3 % of the physiological plasminogen concentration at ~2 μM. In addition, the level of contaminating plasmin activity in three different BLAS preparations were less than 0.3 % compared to purified human plasmin.

BLAS suppresses tumor-induced angiogenesis in a mouse DAS model at 0.8 mg kg^{-1} or more. The BLAS derivative lacking sialic acids at the end of the glycosyl chains (asialo-BLAS) shows a significantly reduced activity (less than 1/10 of that of native BLAS) in the DAS angiogenesis model, suggesting a key role of the glycosyl chain(s). Furthermore, removal of the PAN module reduces activity (the anti-angiogenic activity of desPAN-BLAS at 0.8 mg kg^{-1} is not significant compared to the control). Thus, the PAN module may contribute additionally to BLAS activity. Pharmacokinetic advantages may partly explain the high activity of native BLAS. The intravenously injected recombinant angiostatin K1−3, which lacks the PAN module and the glycosyl chain, has been reported to have linear pharmacokinetics with a serum half-life of 20 min in humans [18], whereas BLAS is cleared from the circulation in two phases: with a $t_{1/2}$ of 1.5 ± 0.2 h for the first distribution phase, followed by a $t_{1/2}$ of 23.6 ± 3.9 h for the elimination phase. This hypothesis is supported by the findings that non-glycosylated plasminogen [28] and plasminogen without thePAN module [29] are cleared from the circulation much faster than native plasminogen.

So far, several forms or angiostatins have been identified [30]. Among them, recombinant angiostatins were developed taking advantage of the ease in large-scale production. One of the recombinant angiostatins clinically tested is angiostatin K1−3, which consists of the first to the third kringle domains of plasminogen (amino acids 97–357 of plasminogen (Lys^{78}–V^{338} of the mature
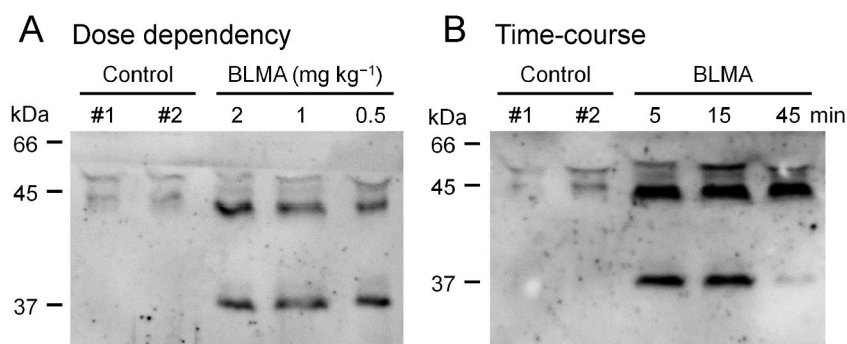
Fig. 8. *In vivo* generation of plasminogen fragments after BLMA injection. C57BL/6 mice received an intravenous injection of BLMA, and plasma levels of plasminogen species were assessed by immunoblotting using an anti-mouse plasminogen antibody. (A) Dose dependence. Mice were treated with the indicated doses of BLMA, and plasma was collected 15 min after injection for evaluation. Control animals received saline. (B) Time course. Mice were treated with BLMA at 2 mg kg^{-1}, and plasma was collected at the indicated time after injection. Control animals received saline, and plasma was collected 15 min after injection. Representative results are shown. Uncropped gel images are provided as supplementary materials (Uncropped gel image for Fig. 8A and Uncropped gel image for Fig. 8B).

plasminogen), with an Asn to Glu mutation at position 389 of the mature plasminogen to prevent N-glycosylation [18]. BLAS differs from the angiostatin K1−3 in that it has an N-terminal PAN module, glycosyl chains, and the kringle 4 domain. BLAS suppresses the growth of syngeneic and xenogeneic tumors implanted in mice. The antitumor activity is significant at 0.3 mg kg^{-1} per day in the LLC implantation model. This BLAS activity appears to be 5−333 times more potent than that of recombinant angiostatin K1−3, which has been reported to have antitumor activity at 1.5−50 mg kg^{-1} [18] or as high as at 100 mg kg^{-1} per day in mice [31], with a plasma AUC$_{0−\infty}$ at 50 mg kg^{-1} per day of 3.4 µg h mL^{-1} [18]. The plasma AUC$_{0−\infty}$ of 58.2 $\pm$ 4.1 after a single injection of BLAS in mice at 1 mg kg^{-1} is 856 times higher than that of recombinant angiostatin K1−3 after dose normalization, again emphasizing the pharmacokinetic advantage. BLAS suppresses the growth of primary and metastatic tumors, as does recombinant angiostatin [31], but at a dose as low as 0.3 mg kg^{-1}.

Angiostatins inhibit tumor growth by blocking the proliferation and migration of vascular endothelial cells. Potential molecules targeted by angiostatins include endothelial cell surface F1–F0 ATP synthase, which maintains intracellular pH in the acidic tumor cell environment [12,32]. Angiostatin inhibits cell surface F1–F0 ATP synthase and decreases intracellular pH, inducing endothelial cell apoptosis [32,33]. Alternatively, angiostatin binds to the cell surface $\alpha_v\beta_3$-integrin and inhibits plasmin-induced cell migration [14, 34]. In addition, angiomotin binds and internalize angiostatin to activate focal adhesion kinase [13], which regulates cell motility and adhesion-dependent cell survival [16]. Another potential target of angiostatin is annexin II, which plays a role in the activation of plasminogen to plasmin [15]. Angiostatin competes with plasminogen for binding to annexin II, thereby inhibiting plasmin-mediated effects on the angiogenic, invasive, and metastatic capability of tumors [35]. Although we have not addressed the details of the mechanism of action of BLAS, it may be similar to that reported for angiostatins, since these angiostatin activities appear to be mediated by interaction between the target and kringle domain(s). Indeed, each of the isolated kringles with lysine binding activity show similar inhibition of endothelial cell proliferation and migration [30].

In addition to the effect of angiostatin in modulating endothelial dysfunction [22,23,36,37] and inflammation [26,38–40], recent research has shown a possible link between angiostatin and cognitive function and the development of Alzheimer's disease [24,25,41, 42]. It is therefore tempting to speculate that the use of pharmacokinetically-advantaged BLAS may be beneficial in controlling these conditions as well as suppressing tumor growth and metastasis. In addition, increasing *in vivo* angiostatin generation can be an alternative means to achieve a goal [43,44]. In this context, we tested the BLAS-generating enzyme BLMA for its potential to generate angiostatin in mice. The protein that appeared after BLMA injection had a molecular mass of ~42 kDa, which was smaller than the size of BLAS (50 kDa, calculated from the amino acid sequence) generated using the affinity-capture reactor. Thus, the 42 kD protein produced *in vivo* may be a truncated form of BLAS. One of the most likely configurations of the protein is a desPAN-like form. This is because BLMA can cleave the Leu^{74}−Phe^{75} bond in plasminogen [21]. Our approach to promote *in vivo* angiostatin formation by BLMA treatment is still preliminary and needs to be further developed. For example, there may be a concern for hypoplasminogenemia, resulting from excessive cleavage of plasminogen by BLMA, and nonspecific proteolytic consequence. Although, our preliminary testing suggests that injection of BLMA up to 2 mg kg^{-1} has minimal impact on the level of plasminogen in mice (Fig. S1) and that repeated injections of 2 mg kg^{-1} BLMA, three times a week for two weeks, do not develop any toxic signs, further studies will be required to establish BLMA-mediated angiostatin formation *in vivo*.

In conclusion, our results are encouraging for the use of BLAS not only in cancer treatment but also in the control of dementia, endothelial function, and inflammation associated with various diseases.

Funding

Ethics statement

The experimental procedures complied to the following ethical guidelines: approval number R05-120 by the Tokyo Noko University Animal Experiment Subcommittee; contract numbers 03243, 06211, and 071212 by the institutional review board of the New Drug Research Laboratories; contract numbers P051476, P070023, P071167, and P080420 by the institutional review board of the Panapharm Laboratories; and contract number AE-5085 by the institutional review board of the Daiichi Pure Chemical.

Data availability statement

Data will be made available on request.

CRediT authorship contribution statement

Kosuke Shimizu: Writing – review & editing, Validation, Methodology, Investigation, Formal analysis, Data curation, Conceptualization. **Naoko Nishimura:** Writing – review & editing, Validation, Methodology, Investigation, Formal analysis, Conceptualization. **Taolin Wang:** Writing – review & editing, Validation, Methodology, Investigation. **Tetsuro Yamamoto:** Writing – review & editing, Supervision, Project administration, Funding acquisition, Formal analysis, Conceptualization. **Eriko Suzuki:** Writing – review & editing, Supervision, Project administration, Funding acquisition, Formal analysis. **Keiji Hasumi:** Writing – review & editing, Writing – original draft, Visualization, Validation, Supervision, Project administration, Methodology, Investigation, Funding acquisition, Formal analysis, Data curation, Conceptualization.

Declaration of competing interest

The authors declare the following financial interests/personal relationships which may be considered as potential competing interestsKS was a doctoral course student and an employee of TMS Co. when engaged in this study; NN was an employee of TMS Co. when engaged in this study; TW is a master course student at Tokyo University of Agriculture and Technology. TY is an employee of EPS Innovative Medicine (Japan); ES is an employee of Tokyo University of Agriculture and Technology. KH is an employee of Tokyo University of Agriculture and Technology, and an employee and a shareholder of TMS Co.

Appendix A. Supplementary data

Supplementary data to this article can be found online at https://doi.org/10.1016/j.heliyon.2024.e35232.

References

[1] M.S. O'Reilly, L. Holmgren, Y. Shing, C. Chen, R.A. Rosenthal, M. Moses, W.S. Lane, Y. Cao, E.H. Sage, J. Folkman, Angiostatin: a novel angiogenesis inhibitor that mediates the suppression of metastases by a Lewis lung carcinoma, Cell 79 (1994) 315–328, https://doi.org/10.1016/0092-8674(94)90200-3.

[2] M.S. O'Reilly, L. Holmgren, C. Chen, J. Folkman, Angiostatin induces and sustains dormancy of human primary tumors in mice, Nat. Med. 2 (1996) 689–692, https://doi.org/10.1038/nm0696-689.

[3] M.S. O'Reilly, D. Wiederschain, W.G. Stetler-Stevenson, J. Folkman, M.A. Moses, Regulation of angiostatin production by matrix metalloproteinase-2 in a model of concomitant resistance, J. Biol. Chem. 274 (1999) 29568–29571, https://doi.org/10.1074/jbc.274.41.29568.

[4] L.A. Cornelius, L.C. Nehring, E. Harding, M. Bolanowski, H.G. Welgus, D.K. Kobayashi, R.A. Pierce, S.D. Shapiro, Matrix metalloproteinases generate angiostatin: effects on neovascularization, J. Immunol. 161 (1998) 6845–6852.

[5] M.J. Gorrin Rivas, S. Arii, M. Furutani, T. Harada, M. Mizumoto, H. Nishiyama, J. Fujita, M. Imamura, Expression of human macrophage metalloelastase gene in hepatocellular carcinoma: correlation with angiostatin generation and its clinical significance, Hepatology 28 (1998) 986–993, https://doi.org/10.1002/hep.510280413.

[6] Z. Dong, R. Kumar, X. Yang, I.J. Fidler, Macrophage-derived metalloelastase is responsible for the generation of angiostatin in Lewis lung carcinoma, Cell 88 (1997) 801–810, https://doi.org/10.1016/s0092-8674(00)81926-1.

[7] H.H. Heidtmann, D.M. Nettelbeck, A. Mingels, R. Jäger, H.G. Welker, R.E. Kontermann, Generation of angiostatin-like fragments from plasminogen by prostate-specific antigen, Br. J. Cancer 81 (1999) 1269–1273, https://doi.org/10.1038/sj.bjc.6692167.

[8] A. Bayés, T. Tsetsenis, S. Ventura, J. Vendrell, F.X. Aviles, G. Sotiropoulou, Human kallikrein 6 activity is regulated via an autoproteolytic mechanism of activation/inactivation, Biol. Chem. 385 (2004) 517–524, https://doi.org/10.1515/BC.2004.061.

[9] S. Gately, P. Twardowski, M.S. Stack, D.L. Cundiff, D. Grella, F.J. Castellino, J. Enghild, H.C. Kwaan, F. Lee, R.A. Kramer, et al., The mechanism of cancer-mediated conversion of plasminogen to the angiogenesis inhibitor angiostatin, Proc. Natl. Acad. Sci. U. S. A. 94 (1997) 10868–10872, https://doi.org/10.1073/pnas.94.20.10868.

[10] P. Stathakis, M. Fitzgerald, L.J. Matthias, C.N. Chesterman, P.J. Hogg, Generation of angiostatin by reduction and proteolysis of plasmin. Catalysis by a plasmin reductase secreted by cultured cells, J. Biol. Chem. 272 (1997) 20641–20645, https://doi.org/10.1074/jbc.272.33.20641.

[11] S. Ohyama, T. Harada, T. Chikanishi, Y. Miura, K. Hasumi, Nonlysine-analog plasminogen modulators promote autoproteolytic generation of plasmin(ogen) fragments with angiostatin-like activity, Eur. J. Biochem. 271 (2004) 809–820, https://doi.org/10.1111/j.1432-1033.2004.03985.x.

[12] T.L. Moser, M.S. Stack, I. Asplin, J.J. Enghild, P. Højrup, L. Everitt, S. Hubchak, H.W. Schnaper, S.V. Pizzo, Angiostatin binds ATP synthase on the surface of human endothelial cells, Proc. Natl. Acad. Sci. U. S. A. 96 (1999) 2811–2816, https://doi.org/10.1073/pnas.96.6.2811.

[13] B. Troyanovsky, T. Levchenko, G. Månsson, O. Matvijenko, L. Holmgren, Angiomotin: an angiostatin binding protein that regulates endothelial cell migration and tube formation, J. Cell Biol. 152 (2001) 1247–1254, https://doi.org/10.1083/jcb.152.6.1247.

[14] T. Tarui, L.A. Miles, Y. Takada, Specific interaction of angiostatin with integrin alpha(v)beta(3) in endothelial cells, J. Biol. Chem. 276 (2001) 39562–39568, https://doi.org/10.1074/jbc.M101815200.

[15] G.P. Tuszynski, M.R. Sharma, V.L. Rothman, M.C. Sharma, Angiostatin binds to tyrosine kinase substrate annexin II through the lysine-binding domain in endothelial cells, Microvasc. Res. 64 (2002) 448–462, https://doi.org/10.1006/mvre.2002.2444.

[16] L. Claesson-Welsh, M. Welsh, N. Ito, B. Anand-Apte, S. Soker, B. Zetter, M. O'Reilly, J. Folkman, Angiostatin induces endothelial cell apoptosis and activation of focal adhesion kinase independently of the integrin-binding motif RGD, Proc. Natl. Acad. Sci. U. S. A. 95 (1998) 5579–5583, https://doi.org/10.1073/pnas.95.10.5579.

[17] M. Gonzalez-Gronow, H.E. Grenett, G. Gawdi, S.V. Pizzo, Angiostatin directly inhibits human prostate tumor cell invasion by blocking plasminogen binding to its cellular receptor, CD26. Exp Cell Res 303 (2005) 22–31, https://doi.org/10.1016/j.yexcr.2004.09.008.

[18] L.V. Beerepoot, E.O. Witteveen, G. Groenewegen, W.E. Fogler, B.K. Sim, C. Sidor, B.A. Zonnenberg, F. Schramel, M.F. Gebbink, E.E. Voest, Recombinant human angiostatin by twice-daily subcutaneous injection in advanced cancer: a pharmacokinetic and long-term safety study, Clin. Cancer Res. 9 (2003) 4025–4033.

[19] A. Kurup, C. Lin, D.J. Murry, L. Dobrolecki, D. Estes, C.T. Yiannoutsos, L. Mariano, C. Sidor, R. Hickey, N. Hanna, Recombinant human angiostatin (rhAngiostatin) in combination with paclitaxel and carboplatin in patients with advanced non-small-cell lung cancer: a phase II study from Indiana University, Ann. Oncol. 17 (2006) 97–103, https://doi.org/10.1093/annonc/mdj055.

[20] K. Shimizu, K. Hasumi, Affinity-capture protease reactor for single-step production and purification of antiangiogenic plasminogen fragment from human plasma, Biotechniques 40 (590) (2006) 592–594, https://doi.org/10.2144/000112172.

[21] R. Narasaki, H. Kuribayashi, K. Shimizu, D. Imamura, T. Sato, K. Hasumi, Bacillolysin MA, a novel bacterial metalloproteinase that produces angiostatin-like fragments from plasminogen and activates protease zymogens in the coagulation and fibrinolysis systems, J. Biol. Chem. 280 (2005) 14278–14287, https://doi.org/10.1074/jbc.M500241200.

[22] N. Lund, H. Wieboldt, L. Fischer, N. Muschol, F. Braun, T. Huber, D. Sorriento, G. Iaccarino, K. Müllerleile, E. Tahir, et al., Overexpression of VEGFα as a biomarker of endothelial dysfunction in aortic tissue of α-GAL-Tg/KO mice and its upregulation in the serum of patients with Fabry's disease, Front Cardiovasc Med 11 (2024) 1355033, https://doi.org/10.3389/fcvm.2024.1355033.

[23] A. Łuczak, R. Małecki, M. Kulus, M. Madej, E. Szahidewicz-Krupska, A. Doroszko, Cardiovascular risk and endothelial dysfunction in primary sjogren syndrome is related to the disease activity, Nutrients 13 (2021), https://doi.org/10.3390/nu13062072.

[24] K.A. Walker, J. Chen, J. Zhang, M. Fornage, Y. Yang, L. Zhou, M.E. Grams, A. Tin, N. Daya, R.C. Hoogeveen, et al., Large-scale plasma proteomic analysis identifies proteins and pathways associated with dementia risk, Nat Aging 1 (2021) 473–489, https://doi.org/10.1038/s43587-021-00064-0.

[25] A. Zarezadehmehrizi, J. Hong, J. Lee, H. Rajabi, R. Gharakhanlu, N. Naghdi, M. Azimi, Y. Park, Exercise training ameliorates cognitive dysfunction in amyloid beta-injected rat model: possible mechanisms of Angiostatin/VEGF signaling, Metab. Brain Dis. 36 (2021) 2263–2271, https://doi.org/10.1007/s11011-021-00751-2.

[26] P.H. Lee, S. Choi, M. An, D. Hwang, S. Park, A.R. Baek, A.S. Jang, Angiomotin and angiostatin as asthma biomarkers: implications for the regulation of airway remodeling and inflammation, Allergy 78 (2023) 1674–1677, https://doi.org/10.1111/all.15637.

[27] K. Ichikawa, T. Hikita, N. Maeda, S. Yonezawa, Y. Takeuchi, T. Asai, Y. Namba, N. Oku, Antiangiogenic photodynamic therapy (PDT) by using long-circulating liposomes modified with peptide specific to angiogenic vessels, Biochim. Biophys. Acta 1669 (2005) 69–74, https://doi.org/10.1016/j.bbamem.2005.02.003.

[28] M. Gonzalez-Gronow, H.E. Grenett, G.M. Fuller, S.V. Pizzo, The role of carbohydrate in the function of human plasminogen: comparison of the protein obtained from molecular cloning and expression in Escherichia coli and COS cells, Biochim. Biophys. Acta 1039 (1990) 269–276, https://doi.org/10.1016/0167-4838(90)90259-i.

[29] C. Miyashita, P. Hellstern, M. Köhler, G. von Blohn, E. Wenzel, In vitro characterization of commercial Factor VIII concentrates: long-term follow-up, Blut 49 (1984) 53–59, https://doi.org/10.1007/BF00320384.

[30] J.H. Geiger, S.E. Cnudde, What the structure of angiostatin may tell us about its mechanism of action, J. Thromb. Haemostasis 2 (2004) 23–34, https://doi.org/10.1111/j.1538-7836.2004.00544.x.

[31] B.K. Sim, M.S. O'Reilly, H. Liang, A.H. Fortier, W. He, J.W. Madsen, R. Lapcevich, C.A. Nacy, A recombinant human angiostatin protein inhibits experimental primary and metastatic cancer, Cancer Res. 57 (1997) 1329–1334.

[32] T.L. Moser, D.J. Kenan, T.A. Ashley, J.A. Roy, M.D. Goodman, U.K. Misra, D.J. Cheek, S.V. Pizzo, Endothelial cell surface F1-F0 ATP synthase is active in ATP synthesis and is inhibited by angiostatin, Proc. Natl. Acad. Sci. U. S. A. 98 (2001) 6656–6661, https://doi.org/10.1073/pnas.131067798.

[33] T.L. Moser, M.S. Stack, M.L. Wahl, S.V. Pizzo, The mechanism of action of angiostatin: can you teach an old dog new tricks? Thromb. Haemostasis 87 (2002) 394–401.

[34] T. Tarui, M. Majumdar, L.A. Miles, W. Ruf, Y. Takada, Plasmin-induced migration of endothelial cells. A potential target for the anti-angiogenic action of angiostatin, J. Biol. Chem. 277 (2002) 33564–33570, https://doi.org/10.1074/jbc.M205514200.

[35] M.C. Sharma, M. Sharma, The role of annexin II in angiogenesis and tumor progression: a potential therapeutic target, Curr. Pharmaceut. Des. 13 (2007) 3568–3575, https://doi.org/10.2174/138161207782794167.

[36] J. Loso, N. Lund, M. Avanesov, N. Muschol, S. Lezius, K. Cordts, E. Schwedhelm, M. Patten, Serum biomarkers of endothelial dysfunction in fabry associated cardiomyopathy, Front Cardiovasc Med 5 (2018) 108, https://doi.org/10.3389/fcvm.2018.00108.

[37] Y. Kanno, The role of fibrinolytic regulators in vascular dysfunction of systemic sclerosis, Int. J. Mol. Sci. 20 (2019), https://doi.org/10.3390/ijms20030619.

[38] R. Benelli, M. Morini, F. Carrozzino, N. Ferrari, S. Minghelli, L. Santi, M. Cassatella, D.M. Noonan, A. Albini, Neutrophils as a key cellular target for angiostatin: implications for regulation of angiogenesis and inflammation, Faseb. J. 16 (2002) 267–269, https://doi.org/10.1096/fj.01-0651fje.

[39] T. Chavakis, A. Athanasopoulos, J.S. Rhee, V. Orlova, T. Schmidt-Wöll, A. Bierhaus, A.E. May, I. Celik, P.P. Nawroth, K.T. Preissner, Angiostatin is a novel anti-inflammatory factor by inhibiting leukocyte recruitment, Blood 105 (2005) 1036–1043, https://doi.org/10.1182/blood-2004-01-0166.

[40] P.C. Chang, H.L. Wu, H.C. Lin, K.C. Wang, G.Y. Shi, Human plasminogen kringle 1-5 reduces atherosclerosis and neointima formation in mice by suppressing the inflammatory signaling pathway, J. Thromb. Haemostasis 8 (2010) 194–201, https://doi.org/10.1111/j.1538-7836.2009.03671.x.

[41] J.K. Ryu, J.P. Little, A. Klegeris, N. Jantaratnotai, J.G. McLarnon, Actions of the anti-angiogenic compound angiostatin in an animal model of Alzheimer's disease, Curr. Alzheimer Res. 10 (2013) 252–260, https://doi.org/10.2174/1567205011310030004.

[42] Y. Cheng, J.R. Ren, J.M. Jian, C.Y. He, M.Y. Xu, G.H. Zeng, C.R. Tan, Y.Y. Shen, W.S. Jin, D.W. Chen, et al., Associations of plasma angiostatin and amyloid-β and tau levels in Alzheimer's disease, Transl. Psychiatry 12 (2022) 194, https://doi.org/10.1038/s41398-022-01962-6.

[43] G.A. Soff, H. Wang, D.L. Cundiff, K. Jiang, B. Martone, A.W. Rademaker, J.A. Doll, T.M. Kuzel, In vivo generation of angiostatin isoforms by administration of a plasminogen activator and a free sulfhydryl donor: a phase I study of an angiostatic cocktail of tissue plasminogen activator and mesna, Clin. Cancer Res. 11 (2005) 6218–6225, https://doi.org/10.1158/1078-0432.CCR-04-1514.

[44] K. Hiramoto, Y. Yamate, Tranexamic acid reduces endometrial cancer effects through the production of angiostatin, J. Cancer 13 (2022) 1603–1610, https://doi.org/10.7150/jca.68169.

[45] F. Duan, S. Simeone, R. Wu, J. Grady, I. Mandoiu, P.K. Srivastava, Area under the curve as a tool to measure kinetics of tumor growth in experimental animals, J. Immunol. Methods 382 (2012) 224–228, https://doi.org/10.1016/j.jim.2012.06.005.